FAR-END CROSSTALK IN ITERATIVELY DETECTED MIMO-OFDM TWISTED PAIR TRANSMISSION SYSTEMS

Andreas Ahrens
Hochschule Wismar, University of Technology, Business and Design
Department of Electrical Engineering and Computer Science, Philipp-Müller-Straße 14, 23966 Wismar, Germany

Christoph Lange
T-Systems Enterprise Services GmbH, Goslarer Ufer 35, 10589 Berlin, Germany

Keywords: Twisted-pair Cable, OFDM, Singular-Value Decomposition, Multiple Input Multiple Output System, Iterative Decoding, EXIT Charts.

Abstract: Crosstalk between neighbouring wire pairs in multi-pair copper cables is an important disturbance, which essentially limits the transmission quality and the throughput of such cables. For high-rate transmission, often the strong near-end crosstalk (NEXT) disturbance is avoided or suppressed and only the far-end crosstalk (FEXT) remains as crosstalk influence. In this contribution the effect of far-end crosstalk (FEXT) in iteratively detected MIMO-OFDM transmission schemes is studied. EXIT (extrinsic information transfer) charts are used for analyzing and optimizing the convergence behaviour of the iterative demapping and decoding.

1 INTRODUCTION

The local cable network substantially ensures the fixed subscriber access to telephone and data services. For the most parts this fixed access network consists of multi-pair symmetric copper cables, where based on electromagnetic coupling, electrical energy passes over from one wire pair to adjacent ones and crosstalk arises, if the signals in the distinct wire pairs lie in the same or at least in overlapping frequency ranges (Valenti, 2002). Crosstalk as an electromagnetic coupling between adjacent wire pairs is one of the most limiting disturbances in local cable networks. Thereby near-end crosstalk (NEXT) and far-end crosstalk (FEXT) occur in bidirectional driven cables (Valenti, 2002). Since the NEXT is a very strong disturbance (Valenti, 2002) several techniques have been developed in order to avoid or suppress NEXT (Honig et al., 1990). In this case only the FEXT remains as a crosstalk influence. Often short cables are used in high-data rate systems in fixed access networks, e. g., optical fibre transmission is used up to a street cabinet or a building and the last drop is bridged by copper cables. Interestingly, investigations in (Lange and Ahrens, 2005) have shown that the FEXT impact is much stronger in short cables than in longer ones. Considering cables or cable binders as MIMO (multiple input multiple output) channels, FEXT in multi-pair copper cables can be seen as a possible application for MIMO techniques. From broadband radio transmission channels, it is well-known that MIMO techniques are able to overcome the limiting factor of multipath propagation known from single-carrier transmission schemes (Raleigh and Cioffi, 1998; Raleigh and Jones, 1999).

Powerful coding algorithms are used in wireline transmission systems. As an example it should be mentioned, that in both voiceband modem technology as well as in the latest VDSL2 (very-high rate digital subscriber line) systems (ITU-T Recommendation G.993.2, 2006), trellis-coded modulation is used. Against this background, the novel contribution of this paper is that we illustrate the effect of FEXT in iteratively detected MIMO-OFDM transmission schemes, whereby both the uncoded as well as the coded systems are restricted to support the same user data rate within the same bandwidth. The performance investigations are carried out by computer simulations and confirmed by EXIT (extrinsic information transfer) charts (Brink, 2001).

The remainder of this paper is organized as follows: Section 2 introduces the cable characteristics and in 3 the FEXT impact is analyzed. In 4 the multicarrier MIMO system model is introduced and

Ahrens A. and Lange C. (2008).
FAR-END CROSSTALK IN ITERATIVELY DETECTED MIMO-OFDM TWISTED PAIR TRANSMISSION SYSTEMS.
In *Proceedings of the International Conference on Signal Processing and Multimedia Applications*, pages 39-46
DOI: 10.5220/0001931300390046

the performance metrics are given. The channel encoded MIMO system is introduced in section 5, while the computation of the EXIT transfer function is presented in section 6. The associated performance results are presented and interpreted in Section 7. Finally, section 8 provides our concluding remarks.

2 CABLE CHARACTERISTICS

The distorting influence of the cable on the wanted signal is modelled by the cable transfer function

$$G_{\mathrm{k}}(f) = \mathrm{e}^{-l\sqrt{\mathrm{j}\frac{f}{f_0}}} \quad , \tag{1}$$

where l denotes the cable length (in km) and f_0 represents the characteristic cable frequency (in $\mathrm{MHz}\cdot\mathrm{km}^2$) (Kreß and Krieghoff, 1973).

The far-end crosstalk coupling is covered by the transfer function $G_{\mathrm{F}}(f)$ with

$$|G_{\mathrm{F}}(f)|^2 = K_{\mathrm{F}} \cdot l \cdot f^2 \quad , \tag{2}$$

whereby K_{F} is a coupling constant of the far-end crosstalk, which depends on the cable properties such as the type of isolation, the number of wire pairs and the kind of combination of the wire pairs within the binders (Valenti, 2002; Galli and Kerpez, 2002a; Galli and Kerpez, 2002b).

If the far-end crosstalk from several neighbouring wire pairs is considered, with increasing distance of the disturbing wire pair from the considered pair in a cable the impact of far-end crosstalk decreases. Considering n_{F} FEXT-disturbing wire pairs, in conformity with cable measurements, this behaviour can be modelled by (Valenti, 2002)

$$K_{\mathrm{F}} = n_{\mathrm{F}}^{0.6} \cdot K_{\mathrm{F1}} \quad , \tag{3}$$

where K_{F1} is the FEXT coupling constant for one disturbing wire pair. By (3) it is taken into account, that the wire pairs, which are located farther away from the considered wire pair contribute less to the FEXT disturbance than the wire pairs, which are located closer to the considered wire pair (Kalet and Shamai (Shitz), 1990; Valenti, 2002).

3 FEXT IMPACT

Since in the copper access network on the one hand very short copper cables are used (e. g. in fibre to the cabinet or fibre to the building architectures) and on the other hand also longer copper cables are applied (e. g. in rural areas) it is of interest, how the far-end crosstalk depends on the cable length (Lange and Ahrens, 2005). Therefore at this point the length-dependency of the FEXT is investigated in an exemplary system according to Fig. 1. For simplicity of calculations, this length dependency of the FEXT is investigated by means of a baseband system.

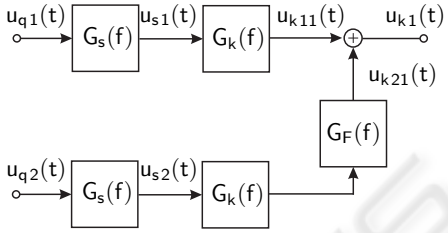

Figure 1: Model of transmitter and cable with FEXT (example: $n = 2$).

It is assumed, that each wire pair within the cable is feeded by a system with identical mean properties with respect to transmit filtering, pulse frequency (or symbol rate) $f_{\mathrm{T}} = 1/T_{\mathrm{s}}$, the number s of signalling levels and the mean transmit power P_{s}[1]. The source signals $u_{\mathrm{q1}}(t)$ and $u_{\mathrm{q2}}(t)$ traverse the transmit filters with the transfer function $G_{\mathrm{s}}(f)$. Then the wanted transmit signal $u_{\mathrm{s1}}(t)$ passes the cable and causes the signal $u_{\mathrm{k11}}(t)$ with power P_{k11} at the cable output, whereas the FEXT signal $u_{\mathrm{k21}}(t)$ (with power P_{k21}) originates at the cable output, after the transmit signal $u_{\mathrm{s2}}(t)$ in the neighbouring wire pair passed through both, the FEXT coupling and the cable transfer function (Fig. 1). The power

$$P_{\mathrm{k11}} = U_{\mathrm{s}}^2 T_{\mathrm{s}} \frac{s^2-1}{3} \int_{-\infty}^{+\infty} |G_{\mathrm{s}}(f) \cdot G_{\mathrm{k}}(f)|^2 \,\mathrm{d}f \tag{4}$$

of the wanted signal $u_{\mathrm{k11}}(t)$ at the cable output decreases monotonically with rising cable length, since with increasing cable length the lowpass effect of the cable $G_{\mathrm{k}}(f)$ becomes stronger and hence the area below $|G_{\mathrm{s}}(f)\cdot G_{\mathrm{k}}(f)|^2$ decreases. From a practical point of view the power

$$P_{\mathrm{k21}} = U_{\mathrm{s}}^2 T_{\mathrm{s}} \frac{s^2-1}{3} \int_{-\infty}^{+\infty} |G_{\mathrm{s}}(f) \cdot G_{\mathrm{F}}(f) \cdot G_{\mathrm{k}}(f)|^2 \,\mathrm{d}f \tag{5}$$

of the FEXT signal $u_{\mathrm{k21}}(t)$ at the cable output ($n_{\mathrm{F}} = 1$) is an interesting indicator for the strength of the FEXT disturbance. In general, this FEXT power depends on the frequency (i. e. signal bandwidth) and on the cable length, because $G_{\mathrm{k}}(f)$ and $G_{\mathrm{F}}(f)$ are functions of the frequency f and of the cable length l. Figure 2 shows

[1] In this contribution a power with the dimension (voltage)^2 (in V^2) is used. At a real, constant resistor this value is proportional to the physical power (in W).

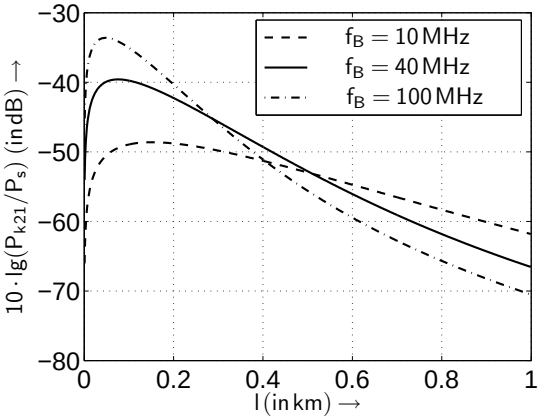

Figure 2: FEXT power P_{k21} at the cable output as a function of the cable length l (parameter: f_B).

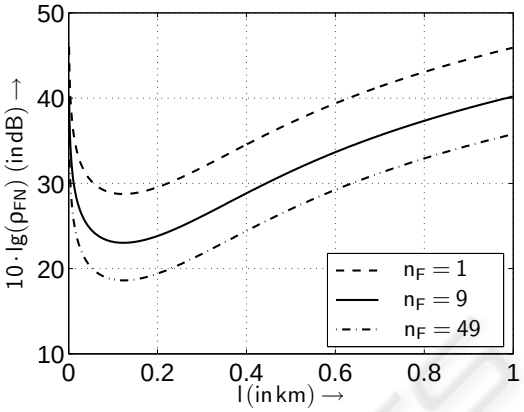

Figure 3: Signal-to-FEXT-interference ratio ρ_{FN} as a function of the cable length l (parameter: n_F).

the mean FEXT power (5) at the cable output depending on the cable length l with root-raised cosine transmit filtering (roll-off factor $r = 0.5$) (Proakis, 2000) and the exemplary parameters $P_s = 1\,\mathrm{V}^2$, $s = 2$ and $K_{F1} = 2.6248 \cdot 10^{-17}\,(\mathrm{Hz}^2 \cdot \mathrm{km})^{-1}$ for different bit rates $f_B = f_T \cdot \log_2(s)$. At a fixed bit rate (fixed required bandwidth) the FEXT power P_{k21} only depends on the cable length l. At very small cable lengths firstly the FEXT power increases, since the FEXT coupling according to (2) rises with increasing cable length l. A maximum in the FEXT power arises at relatively low cable lengths (below 0.2 km), because the FEXT power according to (5) via $G_F(f)$ rises with increasing l and over $G_k(f)$ it decreases with increasing cable length l, i. e., there is a dependency of the FEXT power (5) on the cable length in a opposite direction. At high symbol rates the transmit spectrum is getting broader and this causes a higher maximum in the FEXT power compared to lower pulse frequencies (smaller bandwidth), because the FEXT coupling (2) rises with frequency. The cable length, at which the maximum occurs, decreases with increasing bit rate (increasing bandwidth of the signal), because the lowpass impact of the cable takes already a higher effect on a shorter cable.

In order to assess the effect of far-end crosstalk on the wanted signal not only the pure FEXT signal power is of interest, but rather the behaviour of the powers of the wanted signal and the FEXT signal to each other. This behaviour may be investigated by a signal-to-FEXT-interference ratio (SFIR)

$$\rho_{FN} = \frac{\int_{-\infty}^{+\infty} |G_s(f) \cdot G_k(f)|^2 \,\mathrm{d}f}{\int_{-\infty}^{+\infty} |G_s(f) \cdot G_F(f) \cdot G_k(f)|^2 \,\mathrm{d}f} \qquad (6)$$

with modified FEXT coupling constants K_F according to the number n_F of disturbing wire pairs in $G_F(f)$ described in (3). Figure 3 shows the SFIR ρ_{FN} as a function of the cable length at a fixed bit rate of $f_B = 100\,\mathrm{MHz}$ (and $P_s = 1\,\mathrm{V}^2$, $s = 2$) for different numbers $n_F = n - 1$ of disturbing wire pairs. With increasing number n_F of disturbers the FEXT power increases and therefore the SFIR decreases. Since the FEXT power (5) has a local maximum and the wanted signal power (4) decreases monotonically with respect to the cable length l, a minimum occurs in the SFIR function according to (6).

In particular for short cables the FEXT impact is very significant. Therefore especially in the case, where short copper cables are used the exploitation of FEXT may be useful in order to improve the transmission quality.

4 MIMO-OFDM SYSTEM MODEL

Now a whole cable binder is considered as a transmission channel with multiple inputs and multiple outputs (MIMO). The considered cable binder consists of n wire pairs and therefore a (n, n) MIMO transmission system arises. The mapping of the transmit signals $u_{s\mu}(t)$ onto the received signals $u_{k\mu}(t)$ (with $\mu = 1, \ldots, n$) can be described accordingly to Fig. 4. On each wire pair of the cable binder OFDM (orthogonal frequency division multiplexing) is used as transmission technique to combat the effects of the frequency-selective channel (Bahai and Saltzberg, 1999; Bingham, 2000). In such a (n,n)-MIMO-OFDM system, an N-point IFFT (N subchannels) modulated data signal is transmitted on every wire pair. The system is modelled by

$$\mathbf{u} = \mathbf{R} \cdot \mathbf{c} + \mathbf{w} \ . \qquad (7)$$

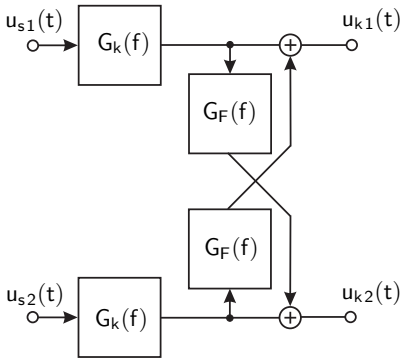

Figure 4: MIMO cable transmission model system with FEXT ($n = 2$).

In (7), $\mathbf{c}$ is the $(L \times 1)$ transmitted signal vector containing the $L = N\,n$ complex input symbols transmitted over all n wire pairs. Using OFDM with a sufficient guard interval length, only symbols that are transmitted over the same subcarrier can interfere each other. The data vector $\mathbf{c}$ can be decomposed according to

$$\mathbf{c} = \left(\mathbf{c}_1^{\mathrm{T}}, \ldots, \mathbf{c}_\kappa^{\mathrm{T}}, \ldots, \mathbf{c}_N^{\mathrm{T}}\right)^{\mathrm{T}} \quad , \tag{8}$$

where the $(n \times 1)$ vector $\mathbf{c}_\kappa$ contains the complex input symbols transmitted over the κth subcarrier on each wire pair. Furthermore $\mathbf{u}$ describes the $(L \times 1)$ received vector and $\mathbf{w}$ is the $(L \times 1)$ vector of the Additive, White Gaussian Noise (AWGN) having a variance of U_{R}^2 for both the real and imaginary parts. Applying OFDM with a sufficient guard interval length, the matrix $\mathbf{R}$ in (7) gets a block diagonal structure according to

$$\mathbf{R} = \begin{bmatrix} \mathbf{R}_1 & \mathbf{0} & \cdots & \mathbf{0} \\ \mathbf{0} & \mathbf{R}_2 & \ddots & \vdots \\ \vdots & \ddots & \ddots & \vdots \\ \mathbf{0} & \mathbf{0} & \cdots & \mathbf{R}_N \end{bmatrix} \quad . \tag{9}$$

In equation (9) zero-matrices are denoted by $\mathbf{0}$ and for the matrices $\mathbf{R}_\kappa$ (with $\kappa = 1, \ldots, N$) the following syntax is used

$$\mathbf{R}_\kappa = \begin{bmatrix} r_{11}^{(\kappa)} & \cdots & r_{1n}^{(\kappa)} \\ \vdots & \ddots & \vdots \\ r_{n1}^{(\kappa)} & \cdots & r_{nn}^{(\kappa)} \end{bmatrix} \quad , \tag{10}$$

with the elements describing the couplings of the data symbols on the subchannel κ. Based on the symmetry of the considered transmission system $r_{\nu\mu}^{(\kappa)}$ (for $\nu = \mu$) can be determined taking the FFT of $g_{\mathrm{k}}(t) = \mathcal{F}^{-1}\{G_{\mathrm{k}}(f)\}$ into account. The elements $r_{\nu\mu}^{(\kappa)}$ (for $\nu \neq \mu$) consider the coupling between neighbouring wire pairs and can be ascertained calculating the FFT of $g_{\mathrm{kfn}}(t) = \mathcal{F}^{-1}\{G_{\mathrm{F}}(f) \cdot G_{\mathrm{k}}(f)\}$. The κth value of this vector represents $r_{\nu\mu}^{(\kappa)}$. The elements $r_{\nu\mu}^{(\kappa)}$ (for $\nu \neq \mu$) are assumed to be identical for each κ, although in practical systems the coupling between the wire pairs is slightly different and it depends on their arrangement in the binder (Valenti, 2002). The subcarrier-specific interferences introduced by the non-diagonal matrix $\mathbf{R}_\kappa$ require appropriate signal processing strategies. A popular technique is based on the SVD of the matrix $\mathbf{R}_\kappa$, which can be written as $\mathbf{R}_\kappa = \mathbf{S}_\kappa \cdot \mathbf{V}_\kappa \cdot \mathbf{D}_\kappa^{\mathrm{H}}$, where $\mathbf{S}_\kappa$ and $\mathbf{D}_\kappa^{\mathrm{H}}$ are unitary matrices and $\mathbf{V}_\kappa$ is a real-valued diagonal matrix of the positive square roots of the eigenvalues of the matrix $\mathbf{R}_\kappa^{\mathrm{H}}\mathbf{R}_\kappa$ sorted in descending order[2]. Using $\mathbf{D}_\kappa$ as preprocessing matrix at the transmitter and $\mathbf{S}_\kappa^{\mathrm{H}}$ as postprocessing matrix at the receiver side, the overall transmission relationship results in

$$\mathbf{y}_\kappa = \mathbf{S}_\kappa^{\mathrm{H}}\left(\mathbf{R}_\kappa \cdot \mathbf{D}_\kappa \cdot \mathbf{c}_\kappa + \mathbf{w}_\kappa\right) = \mathbf{V}_\kappa \cdot \mathbf{c}_\kappa + \tilde{\mathbf{w}}_\kappa . \tag{11}$$

Here, the $(n \times n)$ matrix $\mathbf{R}_\kappa$ is transformed into n independent, non-interfering layers having unequal gains. Arranging the subcarrier specific received vectors $\mathbf{y}_\kappa$ according to (8), leads to the following description of the transmission system according to

$$\mathbf{y} = \mathbf{V} \cdot \mathbf{c} + \tilde{\mathbf{w}} . \tag{12}$$

Therein the $(L \times L)$ matrix $\mathbf{V}$ has a block-diagonal structure according to

$$\mathbf{V} = \begin{bmatrix} \mathbf{V}_1 & \mathbf{0} & \cdots & \mathbf{0} \\ \mathbf{0} & \mathbf{V}_2 & \ddots & \vdots \\ \vdots & \ddots & \ddots & \vdots \\ \mathbf{0} & \mathbf{0} & \cdots & \mathbf{V}_N \end{bmatrix} \quad . \tag{13}$$

Based on the diagonal structure of the subcarrier specific $(n \times n)$ matrices $\mathbf{V}_\kappa$, the channel matrix $\mathbf{R}$ is decomposed into $L = N\,n$ independent, non-interfering layers having unequal gains.

In general, the quality of data transmission can be informally assessed by using the signal-to-noise ratio (SNR) at the detector's input defined by the half vertical eye opening and the noise power per quadrature component according to

$$\rho = \frac{(\text{Half vertical eye opening})^2}{\text{Noise Power}} = \frac{(U_{\mathrm{A}})^2}{(U_{\mathrm{R}})^2} \quad , \tag{14}$$

which is often used as a quality parameter (Ahrens and Lange, 2006). The relationship between the signal-to-noise ratio $\rho = U_{\mathrm{A}}^2/U_{\mathrm{R}}^2$ and the bit-error probability evaluated for AWGN channels and M-ary

[2]The transpose and conjugate transpose (Hermitian) of $\mathbf{D}_\kappa$ are denoted by $\mathbf{D}_\kappa^{\mathrm{T}}$ and $\mathbf{D}_\kappa^{\mathrm{H}}$, respectively.

Quadrature Amplitude Modulation (QAM) is given by (Kalet, 1987; Proakis, 2000)

$$P_{\mathrm{BER}} = \frac{2}{\log_2(M)}\left(1-\frac{1}{\sqrt{M}}\right)\operatorname{erfc}\left(\sqrt{\frac{\rho}{2}}\right) \quad . \quad (15)$$

When applying the proposed system structure, the SVD-based equalization leads to different eye openings per layer ℓ according to

$$U_{\mathrm{A}}^{(\ell)} = \sqrt{\xi_\ell}\cdot U_{\mathrm{s}\ell} \quad , \quad (16)$$

where $U_{\mathrm{s}\ell}$ denotes the half-level transmit amplitude assuming M_ℓ-ary QAM and $\sqrt{\xi_\ell}$ represents the weighting factor (singular value) resulting from the subcarrier-based equalization. Together with the noise power per quadrature component, the SNR per layer becomes

$$\rho^{(\ell)} = \frac{\left(U_{\mathrm{A}}^{(\ell)}\right)^2}{U_{\mathrm{R}}^2} = \xi_\ell \frac{(U_{\mathrm{s}\ell})^2}{U_{\mathrm{R}}^2} \quad . \quad (17)$$

The bit-error probability per layer ℓ is given by (Ahrens and Lange, 2006)

$$P_{\mathrm{BER}}^{(\ell)} = \frac{2\left(1-\frac{1}{\sqrt{M_\ell}}\right)}{\log_2(M_\ell)}\operatorname{erfc}\left(\sqrt{\frac{\xi_\ell}{2}}\cdot\frac{U_{\mathrm{s}\ell}}{U_{\mathrm{R}}}\right) \quad . \quad (18)$$

The resulting average bit-error probability assuming different QAM constellation sizes results in

$$P_{\mathrm{BER}} = \frac{1}{\sum_{\nu=1}^{L}\log_2(M_\nu)}\sum_{\ell=1}^{L}\log_2(M_\ell)\,P_{\mathrm{BER}}^{(\ell)} \quad . \quad (19)$$

Therein the number of transmitted bits per data block results in

$$R = \sum_{\ell=1}^{L}\log_2 M_\ell \quad , \quad (20)$$

assuming that all L layers are used for the data transmission. Considering QAM constellations, the average transmit power $P_{\mathrm{s}\ell}$ per layer ℓ may be expressed as (Forney et al., 1984; Kalet, 1989)

$$P_{\mathrm{s}\ell} = \frac{2}{3}U_{\mathrm{s}\ell}^2(M_\ell-1) \quad . \quad (21)$$

Combining (17) and (21), the layer-specific SNR results in

$$\rho^{(\ell)} = \xi_\ell \frac{3}{2(M_\ell-1)}\frac{P_{\mathrm{s}\ell}}{U_{\mathrm{R}}^2} \quad . \quad (22)$$

Using a parallel transmission over N subchannels the overall mean transmit power per wire yields to

$$P_{\mathrm{s}} = N\cdot P_{\mathrm{s}\ell} = N\frac{2}{3}U_{\mathrm{s}\ell}^2(M_\ell-1) \quad , \quad (23)$$

and results in a total transmit power of nP_{s} by taking n wire-pairs into account. Assuming that the transmit power is uniformly distributed over the number of activated layers per wire, i. e., $P_{\mathrm{s}\ell} = P_{\mathrm{s}}/N$, the half-level transmit amplitude $U_{\mathrm{s}\ell}$ per layer results in

$$U_{\mathrm{s}\ell} = \sqrt{\frac{3P_{\mathrm{s}}}{2N(M_\ell-1)}} \quad . \quad (24)$$

The signal-to-noise ratio per layer ℓ, defined in (17), results together with (24) in

$$\rho^{(\ell)} = \xi_\ell \frac{3}{2N(M_\ell-1)}\frac{P_{\mathrm{s}}}{U_{\mathrm{R}}^2} \quad . \quad (25)$$

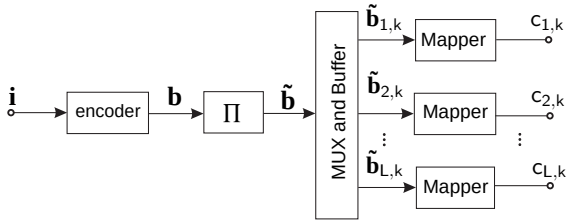

Figure 5: The channel-encoded MIMO-OFDM transmitter structure.

5 CODED MIMO-OFDM SYSTEM

The transmitter structure including channel coding is depicted in Fig. 5. The encoder employs a rate $1/4$ non-recursive, non-systematic convolutional (NSC) code using the generator polynomials $(7,7,7,5)$ in octal notation. The uncoded information is organized in blocks of N_{i} bits, consisting of at least 1000 bits, depending on the specific QAM constellation used. Each data block $\mathbf{i}$ is encoded and results in the block $\mathbf{b}$ consisting of $N_{\mathrm{b}} = 2N_{\mathrm{i}}+8$ encoded bits, including 2 termination bits. The encoded bits are interleaved using a random interleaver and stored in the vector $\tilde{\mathbf{b}}$. The encoded and interleaved bits are then mapped onto the layers. The task of the multiplexer and buffer block of Fig. 5 is to divide the vector of encoded and interleaved information bits $\tilde{\mathbf{b}}$ into subvectors $(\tilde{\mathbf{b}}_{1,k},\tilde{\mathbf{b}}_{2,k},\cdots,\tilde{\mathbf{b}}_{L,k})$, each consisting of R bits according to the chosen throughput. The individual binary data vectors $\tilde{\mathbf{b}}_{\ell,k}$ are then mapped to the QAM symbols $c_{\ell,k}$ according to the specific mapper used. The iterative demodulator structure is shown in Fig. 6. When using the iteration index ν, the first iteration of $\nu=1$ commences with the soft-demapper delivering the N_{b} log-likelihood ratios (LLRs) $L_2^{(\nu=1)}(\tilde{\mathbf{b}})$ of the encoded and interleaved information bits, whose deinterleaved version $L_{\mathrm{a},1}^{(\nu=1)}(\mathbf{b})$ represents the input of the convolutional decoder as depicted in Fig. 6. This channel decoder provides the estimates of the original uncoded information bits, i. e. $L_1^{(\nu=1)}(\mathbf{i})$, as well

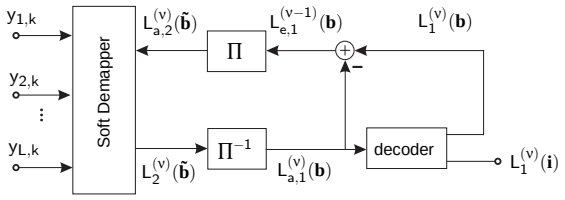

Figure 6: Iterative demodulator structure.

as the LLRs of the N_b NSC-encoded bits in the form of

$$L_1^{(\nu=1)}(\mathbf{b}) = L_{\mathrm{a},1}^{(\nu=1)}(\mathbf{b}) + L_{\mathrm{e},1}^{(\nu=1)}(\mathbf{b}) \ . \qquad (26)$$

As seen in Fig. 6 and Eq. (26), the LLRs of the NSC-encoded bits consist of the receiver's input signal itself plus the extrinsic information $L_{\mathrm{e},1}^{(\nu=1)}(\mathbf{b})$, which is generated by subtracting $L_{\mathrm{a},1}^{(\nu=1)}(\mathbf{b})$ from $L_1^{(\nu=1)}(\mathbf{b})$. The appropriately ordered, i. e. interleaved extrinsic LLRs are fed back as *a priori* information $L_{\mathrm{a},2}^{(\nu=2)}(\tilde{\mathbf{b}})$ to the soft demapper of Fig. 6 for the second iteration. The N_b LLRs $L_2^{(\nu)}(\tilde{\mathbf{b}})$ are composed of the subvectors $(L_2^{(\nu)}(\tilde{\mathbf{b}}_{1,k}), L_2^{(\nu)}(\tilde{\mathbf{b}}_{2,k}), \cdots, L_2^{(\nu)}(\tilde{\mathbf{b}}_{L,k}))$, each consisting of R elements according to the chosen throughput. Each vector $L_2^{(\nu)}(\tilde{\mathbf{b}}_{\ell,k})$ is generated by the soft demapper from the MIMO channel's output $y_{\ell,k}$ and the *a-priori* information $L_{\mathrm{a},2}^{(\nu)}(\tilde{\mathbf{b}}_{\ell,k})$ provided by the channel decoder. After the first iteration, this *a-priori* information emerges from the N_b LLRs $L_{\mathrm{a},2}^{(\nu)}(\tilde{\mathbf{b}})$, which are again decomposed into the subvectors $(L_{\mathrm{a},2}^{(\nu)}(\tilde{\mathbf{b}}_{1,k}), L_{\mathrm{a},2}^{(\nu)}(\tilde{\mathbf{b}}_{2,k}), \cdots, L_{\mathrm{a},2}^{(\nu)}(\tilde{\mathbf{b}}_{L,k}))$, each consisting of R elements.

6 EXIT CHART

The transmitted data sequence $\boldsymbol{B}$ is multiplexed onto the different used layers ℓ and results in the layer specific sequence[3] $\boldsymbol{B}_\ell$ with $\ell = 1, 2, \ldots, L$. The stationary binary input sequence $\boldsymbol{B}_\ell = [B_{\ell,1}, B_{\ell,2}, \ldots, B_{\ell,k}, \ldots]$ consists of r.v.s $B_{\ell,k}$, where the corresponding realizations $b_{\ell,k}$ have an index length of 1 bit and are taken from a finite alphabet $\mathcal{B} = \{0,1\}$ The mapper output sequence $\boldsymbol{C}_\ell = [C_{\ell,1}, C_{\ell,2}, \ldots, C_{\ell,k}, \ldots]$ on the ℓ-th layer consists of r.v.s $C_{\ell,k}$, where the corresponding realizations $c_{\ell,k}$ have an index length of $\log_2(M_\ell)$ bits and are taken from a finite alphabet $\mathcal{C} = \{0, 1, \ldots, M_\ell - 1\}$. The symbols $c_{\ell,k}$ are transmitted over independent channels resulting in the received values $y_{\ell,k}$. The resulting layer-specific model is shown in Fig. 7. The *a priori* channel models the *a priori* information used at the soft demapper. The sequence $\boldsymbol{A}_\ell = [A_{\ell,1}, A_{\ell,2}, \ldots, A_{\ell,k}, \ldots]$ with the corresponding realizations $a_{\ell,k}$ contains the *a priori* LLR information passed to the demapper.

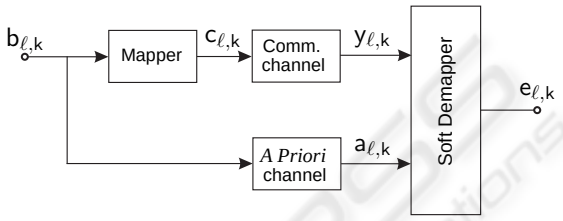

Figure 7: Transmission model analyzing the ℓ-th layer.

EXIT charts visualize the input / output characteristics of the soft demapper and the decoder in terms of a mutual information transfer between the data sequence $\boldsymbol{B}_\ell$ and the sequence $\boldsymbol{A}_\ell$ of the *a priori* LLR information at the input of the soft demapper, as well as between $\boldsymbol{B}_\ell$ and the sequence $\boldsymbol{E}_\ell$ of the extrinsic LLR at the output, respectively. Denoting the mutual information between two r.v.s X and Y as $I(X;Y)$ we may define for a given sequence $\boldsymbol{B}_\ell$ the quantities $I_{\ell,A} = I(\boldsymbol{A}_\ell; \boldsymbol{B}_\ell)$ as well as $I_{\ell,E} = I(\boldsymbol{E}_\ell; \boldsymbol{B}_\ell)$. Herein, $I_{\ell,A}$ represents the average *a priori* information and $I_{\ell,E}$ the average extrinsic information, respectively (Ahrens et al., 2008). The transfer characteristic T of the soft demapper is given by $I_{\ell,E} = T(I_{\ell,A}, \rho)$, where ρ represents the SNR of the communication channel. Analyzing the outer decoder in a serially concatenated scheme T does not depend on ρ. An EXIT chart is now obtained by plotting the transfer characteristics T for both the demapper and the decoder within a single diagram, where the axes have to be swapped for one of the constituent decoders (Brink, 2001) (normally the outer one for serial concatenation).

Transmitting R bits per data block, a layer specific parameter $\alpha^{(\ell)}$ can be defined as follows

$$\alpha^{(\ell)} = \frac{\log_2 M_\ell}{R} \ , \qquad (27)$$

describing the fraction of the data sequence $\boldsymbol{B}$ that is transmitted over the ℓth layer, i. e. $\boldsymbol{B}_\ell$. The mutual information for a given sequence $\boldsymbol{B}$ and the extrinsic LLR $\boldsymbol{E}$ at the output is obtained by

$$I(\boldsymbol{E}; \boldsymbol{B}) = \sum_{\ell=1}^{L} \alpha^{(\ell)} I(\boldsymbol{E}_\ell; \boldsymbol{B}_\ell) \ , \qquad (28)$$

as it was shown in (Ahrens et al., 2008). Hence, the mutual information for a given sequence $\boldsymbol{B}$ and the

[3] Random variables (r.v.s) are denoted with capital letters and their corresponding realizations with lower case letters. Sequences of random variables and realizations are indicated by boldface italics letters (as $\boldsymbol{B}$ or $\boldsymbol{b}$). Furthermore, boldface roman letters denote vectors (as $\mathbf{B}$ or $\mathbf{b}$). The time instant is denoted with k and the layer with ℓ.

extrinsic LLR $\boldsymbol{E}$ is effected by the layer-specific characteristics, i. e. the SNR and the mapping of the bits to both the QAM symbols as well as to the layers, as well as the layer specific parameters $\alpha^{(\ell)}$.

7 RESULTS

The FEXT impact is in particular strong for short cables (Valenti, 2002). Therefore for numerical analysis an exemplary cable of length $l = 0.4\,\mathrm{km}$ with $n = 10$ wire pairs is chosen. The wire diameter is 0.6 mm and hence a characteristic cable frequency of $f_0 = 0.178\,\mathrm{MHz}\cdot\mathrm{km}^2$ is assumed. On each of the wire pairs a multicarrier system with $N = 10$ subcarriers was considered. The actual crosstalk circumstances are difficult to acquire and they vary from cable to cable. Therefore an exemplary mean FEXT coupling constants of $K_\mathrm{F} = 10^{-13}\ldots10^{-15}\,(\mathrm{Hz}^2\cdot\mathrm{km})^{-1}$ are employed (Valenti, 2002; Aslanis and Cioffi, 1992). The average transmit power on each wire pair is supposed to be $P_\mathrm{s} = 1\,\mathrm{V}^2$ and as an external disturbance a white Gaussian noise with power spectral density Ψ_0 is assumed. Identical systems on all wire pairs are presumed (multicarrier symbol duration $T_\mathrm{s} = 2\,\mu\mathrm{s}$, M-ary QAM and a guard interval length of $T_\mathrm{g} = T_\mathrm{s}/2$). Furthermore, the baseband channel of the multicarrier system is excluded from the transmission in order to provide this frequency range for analogue telephone transmission. For a fair comparison the ratio of symbol energy to noise power spectral density at the cable output is defined for the MIMO case $(n > 1)$ according to

$$\frac{E_\mathrm{s}}{\Psi_0} = \left(T_\mathrm{s} + T_\mathrm{g}\right)\frac{P_\mathrm{k} + (n-1)P_\mathrm{kfn}}{\Psi_0}\ , \qquad (29)$$

with P_k as mean power of the signal on the direct paths at the cable output and P_kfn as mean FEXT signal power at the cable output (Ahrens and Lange, 2006). Using the constraint-length $K = 3$ NSC code with the generator polynomials of $(7,7,7,5)$ in octal notation, the performance is analyzed for an effective user throughput of 4 bit/s/Hz. Our results, obtained by analyzing the soft-demapper characteristic (Fig. 8), suggest that the performance of the MIMO-OFDM system is strongly effected by the FEXT coupling. Here it turns out that a heavy FEXT coupling is highly beneficial for a fast convergence in the low SNR region as it is can be seen in Fig. 9. In general, the achievable performance of the iterative decoder is substantially affected by the specific mapping of the bits to both the QAM symbols as well as to the layers. While the employment of the classic Gray-mapping is appropriate in the absence of *a priori* information,

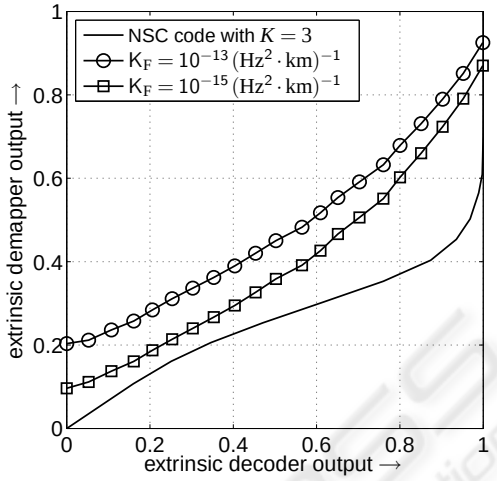

Figure 8: Exit chart with anti-Gray mapping on all activated layers at $10\log_{10}(E_\mathrm{s}/\Psi_0) = 15$ dB.

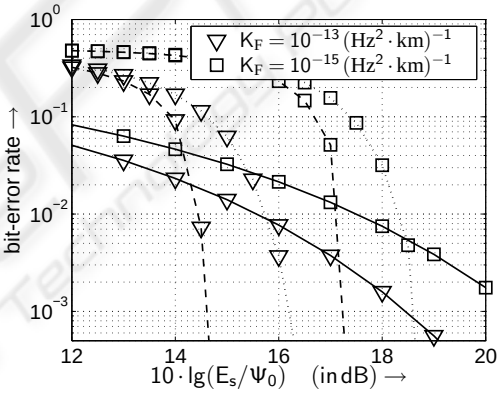

Figure 9: BER of the investigated system (solid line ≙ uncoded system using 4-QAM on all layers, dotted line ≙ iteratively detected coded system (3 iterations) with anti-gray mapping and 16-QAM on all layers, dashed line ≙ iteratively detected coded system (10 iterations) with anti-gray mapping and 16-QAM on all layers).

the availability of *a priori* information in iteratively detecting decoders requires an exhaustive search for finding the best non-Gray – synonymously also referred to as anti-Gray – mapping scheme (Chindapol, 2001). Investigations in (Ahrens et al., 2008) have shown that layer-specific mapping schemes only offer a slightly better performance at low SNRs. Therefore throughout this work anti-gray mapping were used on all layers. Our BER curves obtained by computer simulations show that the overall BER performance is strongly effected by both the FEXT coupling and the number of iterations. Thereby the FEXT coupling between neighbouring wire pairs seems to be a real catalyst for the overall performance that is effected

by both the cable length as well as the cable properties such as the type of isolation, the number of wire pairs and the kind of combination of the wire pairs within the binders.

8 CONCLUSIONS

In this contribution the FEXT impact in iteratively detected MIMO-OFDM transmission schemes has been studied. Our results show that FEXT is not necessarily a limiting factor if appropriate signal processing strategies are used. Our results show that a heavy FEXT impact is overall beneficial for a good convergence behaviour at low SNR. Having hybrid optical and electrical fixed access networks with relatively short copper cables (e. g. fibre transmission up to a street cabinet or a building and bridging the last short drop by already installed twisted pair copper cables), iteratively detected and SVD-aided MIMO-OFDM transmission schemes seems to be a true alternative for delivering broadband services, when heavy FEXT couplings between neighbouring wire pairs can be expected.

REFERENCES

Ahrens, A., Kühn, V., and Weber, T. (2008). Iterative Detection for Spatial Multiplexing with Adaptive Power Allocation. In *7th International Conference on Source and Channel Coding (SCC)*, Ulm.

Ahrens, A. and Lange, C. (2006). Optimal Power Allocation in a MIMO-OFDM Twisted Pair Transmission System with Far-End Crosstalk. In *International Conference on Signal Processing and Multimedia Applications (SIGMAP)*, Setúbal (Portugal).

Aslanis, J. T. and Cioffi, J. M. (1992). Achievable Information Rates on Digital Subscriber Loops: Limiting Information Rates with Crosstalk Noise. *IEEE Transactions on Communications*, 40(2):361–372.

Bahai, A. R. S. and Saltzberg, B. R. (1999). *Multi-Carrier Digital Communications – Theory and Applications of OFDM*. Kluwer Academic/Plenum Publishers, New York, Boston, Dordrecht, London, Moskau.

Bingham, J. A. C. (2000). *ADSL, VDSL, and Multicarrier Modulation*. Wiley, New York.

Brink, S. t. (2001). Convergence Behavior of Iteratively Decoded Parallel Concatenated Codes. *IEEE Transactions on Communications*, 49(10):1727–1737.

Chindapol, A. Ritcey, J. A. (2001). Design, Analysis, and Performance Evaluation for BICM-ID withsquare QAM Constellations in Rayleigh Fading Channels. *IEEE Journal on Selected Areas in Communications*, 19(5):944–957.

Forney, G. D., Gallager, R. G., Lang, G. R., Longstaff, F. M., and Qureshi, S. U. (1984). Efficient Modulation for Band-Limited Channels. *IEEE Journal on Selected Areas in Communications*, 2(5):632–647.

Galli, S. and Kerpez, K. J. (2002a). Methods of Summing Crosstalk From Mixed Sources—Part I: Theoretical Analysis. *IEEE Transactions on Communications*, 50(3):453–461.

Galli, S. and Kerpez, K. J. (2002b). Methods of Summing Crosstalk From Mixed Sources—Part II: Performance Results. *IEEE Transactions on Communications*, 50(4):600–607.

Honig, M. L., Steiglitz, K., and Gopinath, B. (1990). Multichannel Signal Processing for Data Communications in the Presence of Crosstalk. *IEEE Transactions on Communications*, 38(4):551–558.

ITU-T Recommendation G.993.2 (2006). *Very high speed digital subscriber line transceivers 2 (VDSL2)*. International Telecommunication Union, Geneva.

Kalet, I. (1987). Optimization of Linearly Equalized QAM. *IEEE Transactions on Communications*, 35(11):1234–1236.

Kalet, I. (1989). The Multitone Channel. *IEEE Transactions on Communications*, 37(2):119–124.

Kalet, I. and Shamai (Shitz), S. (1990). On the Capacity of a Twisted-Wire Pair: Gaussian Model. *IEEE Transactions on Communications*, 38(3):379–383.

Kreß, D. and Krieghoff, M. (1973). Elementare Approximation und Entzerrung bei der Übertragung von PCM-Signalen über Koaxialkabel. *Nachrichtentechnik Elektronik*, 23(6):225–227.

Lange, C. and Ahrens, A. (2005). Effect of Far-End Crosstalk in Multi-Pair Symmetric Copper Cables. In *XXI Krajowe Sympozjum Telekomunikacji (KST)*, pages 181–190, Bydgoszcz (Poland).

Proakis, J. G. (2000). *Digital Communications*. McGraw-Hill, Boston.

Raleigh, G. G. and Cioffi, J. M. (1998). Spatio-Temporal Coding for Wireless Communication. *IEEE Transactions on Communications*, 46(3):357–366.

Raleigh, G. G. and Jones, V. K. (1999). Multivariate Modulation and Coding for Wireless Communication. *IEEE Journal on Selected Areas in Communications*, 17(5):851–866.

Valenti, C. (2002). NEXT and FEXT Models for Twisted-Pair North American Loop Plant. *IEEE Journal on Selected Areas in Communications*, 20(5):893–900.